Proceedings of IMECE2005
2005 ASME International Mechanical Engineering Congress and Exposition
November 5-11, 2005, Orlando, Florida USA

IMECE2005-79175

DESIGN OPTIMIZATION OF NETWORKS OF COOLING PASSAGES

NENAD JELISAVCIC[1]
Department of Mechanical and Materials Engineering
Multidisciplinary Analysis, Inverse Design, Robust Optimization and Control (MAIDROC) Lab., EC 3474
Florida International University
10555 West Flagler Street, Miami, FL 33174, U.S.A.
njeli001@fiu.edu

THOMAS J. MARTIN[2]
Pratt & Whitney Engine Company
Turbine Discipline Engineering & Optimization Group
M/S 169-20
400 Main Street, East Hartford, CT 06108, U.S.A.
thomas.martin@pw.utc.com

RAMON J. MORAL[3]
Department of Mechanical and Materials Engineering
Multidisciplinary Analysis, Inverse Design, Robust Optimization and Control (MAIDROC) Lab., EC 3474
Florida International University
10555 West Flagler Street, Miami, FL 33174, U.S.A.
rmora022@fiu.edu

DEBASIS SAHOO[4]
Department of Mechanical and Materials Engineering
Multidisciplinary Analysis, Inverse Design, Robust Optimization and Control (MAIDROC) Lab., EC 3474
Florida International University
10555 West Flagler Street, Miami, FL 33174, U.S.A.
dsaho001@fiu.edu

GEORGE S. DULIKRAVICH[5]
Department of Mechanical and Materials Engineering
Multidisciplinary Analysis, Inverse Design, Robust Optimization and Control (MAIDROC) Lab., EC 3474
Florida International University
10555 West Flagler Street, Miami, FL 33174, U.S.A.
dulikrav@fiu.edu Web page: http://maidroc.fiu.edu

MAICKEL GONZALEZ[6]
Department of Mechanical and Materials Engineering
Multidisciplinary Analysis, Inverse Design, Robust Optimization and Control (MAIDROC) Lab., EC 3474
Florida International University
10555 West Flagler Street, Miami, FL 33174, U.S.A.
maickel.gonzalez@fiu.edu

ABSTRACT

A one-dimensional thermo-fluid flow network analysis program COOLNET was developed to predict coolant flow rates, total coolant pressures, bulk coolant total temperatures, and internal heat transfer coefficient distributions, inside internally cooled objects. The coolant passages were allowed to be an arbitrary network of one-dimensional fluid elements or tubes.

Geometric parameters of each passage were optimized using a hybrid multi-objective optimization algorithm. For the chosen Pratt & Whitney gas turbine the cross-sectional areas, hydraulic diameters, ribs' heights and angles in each passage were optimized in order to minimize coolant flow rate, coolant total pressure loss, and total heat removed by coolant from the system. Validation of the hybrid multi-objective optimizer was performed with various test functions. Also, validation of the COOLNET was done with existing Pratt & Whitney gas turbine blade. Program OBJ was written to connect hybrid multi-objective optimizer and COOLNET. Optimization process was visualized using Tecplot (commercial software). Program PLOT was written to write input file for Tecplot, purpose of PLOT was to visualize initial and optimized results. Analysis for the best optimal result is given.

The resulting COOLNET analysis provided coolant flow rates, total and static pressures and temperatures, and the heat transfer coefficient of each fluid element. The COOLNET analysis algorithm would typically converge in 50 iterations requiring about 5 seconds of CPU time on a 3.0 GHz processor. Results demonstrated that in case of an internally cooled gas turbine blade an improvement in overall performance is possible. A typical design optimization required between 500-1,000 iterations with a population of 30 designs. Thus, total number of configurations analyzed was approximately 15,000-30,000.

[1]Graduate student. Student member ASME.
[2] Senior systems design engineer. Member ASME.
[3]Graduate student.
[4]Graduate student.
[5] Professor and Chairman, MME Department.
Director of MAIDROC. Fellow ASME.
[6]Graduate student.

NOMENCLATURE

A	Cross-sectional area of a coolant passage
C_D	Coolant flow discharge coefficient
C_f	Skin friction coefficient in a coolant passage
C_p	Specific heat of coolant
D	Diameter of a coolant passage
D_h	Hydraulic diameter of a coolant passage
e^+	Roughness Reynolds number
f	Friction factor in a coolant passage
$\bar{f}$	Friction factor weighted by area
G	Ideal mass flow rate in a coolant passage
Gc	Coolant mass flow rate
H	Coolant passage height from pressure to suction side
h_c	Heat transfer coefficient on internal surfaces
H_r	Rothalpy
k	Thermal conductivity of the material
M	Local coolant flow Mach number
N_{FE}	Number of fluid elements
N_{FN}	Number of fluid nodes
Nu	Local coolant Nusselt number
Pr	Coolant Prandtl number
P_s	Static pressure in coolant fluid system
P_t	Total pressure in coolant fluid system
Q_c	Heat flux through internal coolant passage surface
r	Radius from the axis of rotation
Re	Reynolds number
S_n	Transverse distance between tube banks
S_p	Longitudinal distance between tube banks
St	Stanton number
T_c	Bulk coolant static temperature
T_{rt}	Relative total temperature of the coolant
T_t	Total temperature
$T_{t,c}$	Bulk total temperature of coolant
v	Average local speed of coolant
W	Coolant passage width from leading to trailing sides

Greek letters

α	Turbulator rib (trip strip) skew angle
ε	Coolant passage wall roughness, trip strip or turbulator height
$\varepsilon_p/\varepsilon$	Trip strip or turbulator pitch-to-height ratio
γ	Ratio of specific heats of coolant
μ	Viscosity coefficient of coolant
ρ	Density of coolant
τ_w	Shear stress at the wall
ω	Iterative relaxation coefficient
Ω	Angular speed of rotation of the cooled object

INTRODUCTION

In many internally cooled configurations it is highly desirable to perform a very fast analysis of arbitrary networks of cooling passages [1] that might contain irregular shapes, surface roughness, and flow turbulators. The cooled objects could also rotate (as in case of internally cooled gas turbine rotor blades [2-8]), could use compressible fluid as a coolant, and could be internally heated with distributed heat sources (as in the case of heating and ventilation of multistory buildings, cruise ships, mine shafts, etc.). The speed of the analysis is of main importance even at the expense of very high accuracy especially in the cases of multi-objective design of branching cooling networks [9] and in the detection of locations and extent of damage to such networks. Consequently, a highly desirable alternative to a very costly fully three-dimensional conjugate heat transfer analysis [10] of such systems is a much faster approximate analysis using a network of quasi-one-dimensional fluid flow elements to model the cooling passages. Such a tool could utilize a wealth of publicly available empirical relations for friction and convective heat transfer in one-dimensional passages [11].

A quasi one-dimensional thermo-fluid flow network analysis COOLNET [2-4] was written in the FORTRAN programming language. Each fluid element had two nodal endpoints. Each internal node needed to have at least one path entering it (source) and one or more paths leaving (sink). Those nodes that had no sources but had one or more sink paths indicated a supply path. Those nodes connected to one or more sources, but having no sink paths were called a dump path (exit). A hybrid optimization algorithm that is capable of dealing with several objective functions simultaneously in a Pareto optimal sense was used to optimize various parameters in COOLNET.

INTERNAL COOLANT NETWORK MODEL

Shape of the internally cooled turbine blade is shown in Figure 1. This object has two inlets and three exits and the main flow path follows a serpentine like passage. In the serpentine there are micro ribs that promote heat transfer. Other features that promote heat transfer (like staggered and inline rows of pin fins and impingement) are part of the code, but are not considered at this time.

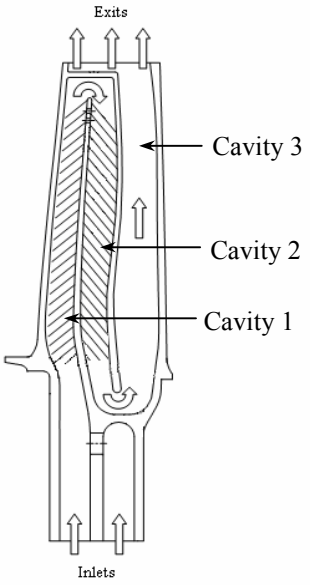

Fig. 1: Cross-section schematic of an internally cooled object (a gas turbine blade) depicting cavities, global direction of coolant flow, turbulator ribs, turn-around sections, inlets and exits

In Figure 2 each node is represented by rectangle and each element is a line connecting two nodes. The coolant flow enters at elements E1 and E2 and exits at elements E46, E47, and E48. The internal coolant network was sub-divided into *kk* elements (fluid paths). Fluid elements were connected as shown in Figure 2 between *nn* nodes. Number of inlet and exit nodes, *mm,* was included in the total number of nodes, *nn*.

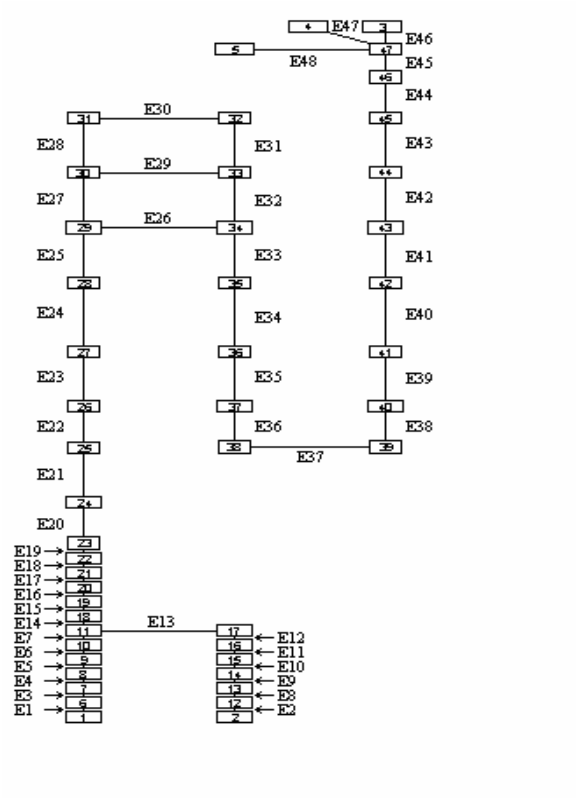

Fig. 2: Coolant passage network model for the internally cooled turbine blade

In this coolant flow passage analysis program, semi-empirical correlations were used to determine the coolant heat transfer coefficients, h_c, while the quasi-one-dimensional momentum and enthalpy equations were solved for the total pressure losses and bulk coolant temperatures, $T_{t,c}$, of the coolant fluid. The heat transfer coefficients and bulk coolant temperatures were assumed to vary in the coolant flow direction. The internal boundary conditions were obtained from a three-dimensional heat conduction model using finite elements.

COOLANT TOTAL PRESSURE AND FLOW BALANCE

Much of the heat transfer was due to high heat transfer coefficients resulting from fully-developed turbulence brought on or enhanced by trip strips and wall roughness. Frictional shear forces cause most of the internal pressure losses, and these can be correlated to the passage length, wall roughness and velocity with a non-linear friction coefficient. Also, inlet losses can have a significant influence on the total losses, especially for rotating passages. When adding banks of pin fins, rows of skewed internal ribs or trip strips, 180^o bends, internal impingements and other heat transfer enhancements, the one-dimensional computational prediction of internal flow losses and coolant heat-up must be correlated with a great deal of empirical data over a broad range of operating conditions, configurations and characteristics. A large number of heat transfer and pressure loss correlations appear in the open literature.

The relative total pressure drop, ΔP_t, across each element that rotates with angular speed Ω, is governed by the momentum conservation equation. Pressure changes due to friction, ΔP_f, acceleration of the flow by heating, ΔP_a, and centrifugal pumping, ΔP_c, are summed up as the total pressure change between nodes 1 and 2 of each fluid element [11].

$$P_{t,2} - P_{t,1} = \Delta P_f + \Delta P_a + \Delta P_c \tag{1}$$

The pressure loss due to friction, ΔP_f, is proportional to the dynamic pressure. The pressure change due to centrifugal pumping, ΔP_c, was derived from the momentum equation. The subsonic fluid accelerates when heat is added, so the pressure change due to heating is included with the addition of the term, ΔP_a. Hence, the three types of the total pressure change are given as

$$\Delta P_f = -C_f \frac{1}{2}\rho v^2 \tag{2a}$$

$$\Delta P_a = \frac{\gamma}{2} M^2 \frac{\left(T_{rt2} - T_{rt1}\right)}{T_{rt}} P_t \tag{2b}$$

$$\Delta P_c = \rho r \Omega^2 \left(r_2 - r_1\right) \tag{2c}$$

When the element was an exit path, the total pressure was related to the static (dump) pressure. In order to model these elements, the friction coefficient was set to unity, $C_f = 1.0$.

A discharge coefficient, C_D, was also needed to determine the actual exit path flow rates. C_D was defined as the ratio of the actual mass flow rate, G, to the ideal mass flow rate. The ideal mass flow rate was calculated by assuming an isentropic one-dimensional expansion from the total pressure, P_t, to the static pressure. P_s.

$$C_D = \frac{G}{P_t\left(\frac{P_s}{P_t}\right)^{\frac{\gamma+1}{2\gamma}} A \sqrt{\frac{2\gamma}{(\gamma-1)rT_t}\left[\left(\frac{P_t}{P_s}\right)^{\frac{\gamma-1}{\gamma}} - 1\right]}} \tag{3}$$

Equation 3 was used to calculate the mass flow rates during the iterative solution procedure. Discharge coefficients were dependent on local coolant passage geometry as well as internal and external flow conditions [12].

The actual mass flow rate of the coolant through the element, G, is an unknown in this system. Continuity gives equilibrium conditions at the nodes of the fluid network. Here, G_m is positive entering the node and negative leaving the node. The summation is over each m^{th} element attached to the node.

$$G = \rho A v \tag{4}$$

$$\sum_m G_m = 0 \tag{5}$$

The N_{FE} elemental pressure balance equations (1) were cast into a local matrix form [11].

$$\begin{bmatrix} \beta & -\beta \\ -\beta & \beta \end{bmatrix} \begin{Bmatrix} P_{in} \\ P_{ex} \end{Bmatrix} = \begin{Bmatrix} G_{in} \\ G_{ex} \end{Bmatrix} + \beta \begin{bmatrix} \Delta P_a + \Delta P_c \\ -\Delta P_a - \Delta P_c \end{bmatrix} \tag{6}$$

where

$$\beta = \frac{2A}{C_f v} \tag{7}$$

Pressure boundary conditions were applied at the inlet and exit (source and sink) nodes of the network. The fluid network was allowed to have an arbitrary number of inlet nodes and exit nodes, although in this case the network consists of two inlets and three exits. The equilibrium equations were written only at the internal nodes since they are not applicable at inlet and exit nodes.

TOTAL ENTHALPY CONSERVATION

The enthalpy conservation equation was used to calculate the bulk coolant total temperatures, $T_{t,c}$, of the convecting and rotating coolant fluid. Convective heat transfer through the walls of the coolant flow passage, Q_c, accounted for heat addition to the coolant. The energy equation for the cooling air was expressed in local finite element matrix form in terms of total rothalpy, H_r.[11]

$$\begin{bmatrix} G & -G \\ -G & G \end{bmatrix} \begin{Bmatrix} H_{r,in} \\ H_{r,ex} \end{Bmatrix} = \begin{Bmatrix} -Q_c \\ Q_c \end{Bmatrix} \tag{8}$$

The total rothalpy per unit mass at each node is defined by

$$H_r = C_p T_c + \frac{1}{2} v^2 - \frac{1}{2} (r\Omega)^2 \tag{9}$$

The heat flux, Q_c, was obtained by a 3-D conjugate heat transfer analysis [10] in the object. The system of equations (8) was generated for each fluid element, assembled into a global system using the FEM [13, 14] and solved with SVD [15]. The solution of this system required that the bulk total temperature of the coolant, $T_{t,c}$, be specified at all inlet paths.

COOLNET ITERATIONS

The thermo-fluid network problem was solved by a finite element algorithm for a specified inlet relative total pressures, inlet relative total temperatures and exit static pressures. The equations were solved by a Picard iteration strategy due to the nonlinearity of the head loss functions. The stability and convergence of the solution technique was dependent upon the accuracy of the initial guess to the mass flow rates in the network. The program allows for an initial guess for *{G}*, but if none is given, the program provides an automatic initialization strategy. This initialization procedure distributes the flow rates by splitting them at each node according to the cross sectional areas of the paths leaving the node. If any path leaving the node is found to be choked, the flow rate of that path is fixed to the choking flow rate. If all paths leaving the node are choked, then the paths entering the node are assumed to be choked, and so on. If COOLNET failed to converge, the design was assumed to be infeasible. The simple iteration was

$$G^{n+1} = (1-\omega) G^n + \omega G^{n+1} \tag{10}$$

The relaxation factor was set initially to $\omega = 0.01$, and it could be increased to about *0.1* once COOLNET reached a reasonable level of convergence. The algorithm would typically take between *10-80* iterations to reach a converged solution, defined as when the flow rates did not change by more than a $1x10^{-6}$ residual. Static variables of pressure, P_s, temperature, T_s density, r, velocity, v, material properties of specific heat, C_p, gas constant, R, viscosity, μ, and thermal conductivity, k, coefficients were determined within each fluid element at each iteration given the total pressure, rothalpy and mass flow rate in each fluid element. Some combinations of these total conditions were impossible indicating a locally choked internal path.

CREATING NETWORK GEOMETRY

Geometric information of the internal coolant passages was accomplished with a COOLNET's ability to read an input deck as a template [2-4]. The geometry-mapping information included the radial variation of the following geometric functions:

1. cross-sectional areas of the cooling passages,
2. perimeters of the passages,
3. cross-sectional heights and widths of the passages,
4. thickness of the ribs on the walls of the passages,
5. diameters and pitch of the impingement holes,
6. length and width of the trailing edge slot, and
7. radial height and pitch of the trailing edge slot.

The geometric information about the axially-flowing passages (tip flag) and the U-turns were mapped with the same utility, but the user needed to supply the streamwise coordinate of the mean coolant fluid path as a function of the axial coordinate, x and the radial distance, r.

FRICTION LOSSES

Various values for friction losses are available in literature. There are different values for friction losses, depending on conditions which are present in the fluid flow.

Friction losses used in COOLNET are briefly presented in Table 1, for more detailed description specified references should be used. The first column, named Type, tells about type of the flow. The second column, named Lit., tells about reference from which given formula was obtained. The third column tells for what purpose the formula is given. The fourth column gives formula and equation number. Shortcut Comm. means comment.

Type	Lit.	Name	Formula and equation number
Smooth wall	[16]	Friction factor	$f = \frac{0.25}{(1.58\ln(Re) - 3.28)^2}$ (11)
		Stanton number	$St = \frac{f/2}{1 + 12.7\left(Pr^{2/3} - 1\right)\sqrt{f/2}}$ (12)
		Comm.	$St = h_c/(\rho C_p v)$ $4C_f = f = 8\tau_w/(\rho v^2)$
Fully developed turbulent flow over rough walls	[17]	Friction factor	$\frac{1}{\sqrt{f}} = -1.8\log\left(\frac{6.9}{Re} + \left(\frac{\varepsilon}{3.7D_h}\right)^{1.11}\right)$ (13)
	[18] [19] [19]	Stanton number	$St = \frac{f/8}{1 + \sqrt{f/8}\left[G\left(e^+\right)Pr^{\varphi} - B\left(e^+\right)\right]}$ (14)
		e^+	$e^+ = \frac{\varepsilon}{D_h} Re_D \sqrt{\frac{f}{8}}$ (15)
Rectangular passages with rblets	[20]	Friction factor	$f = \bar{f} + (H/W)(\bar{f} - f_s)$ (16)
			Smooth $f_s = 0.046\,Re^{-0.2}$ (17)
			Fully developed turbulent flow $f_R = \sqrt{\frac{2}{f}} + 2.5\ln\left[\frac{2\varepsilon}{D_h}\frac{2W}{H+W}\right] + 2.5$ (18) For $e^+ > 50$ $\frac{f_R}{\left(\frac{\varepsilon_p}{10\varepsilon}\right)^{0.35}\left(\frac{W}{H}\right)^m} =$ (19) $= 12.31 - 27.07\left(\frac{\alpha}{90^o}\right) + 17.86\left(\frac{\alpha}{90^o}\right)^2$
		Heat transfer roughness function	Two opposite ribbed walls $H_R = f_R + \frac{\left(\bar{f} + \frac{H}{W}\left(\bar{f} - f_s\right)\right)\Big/2St - 1}{\sqrt{\left[\bar{f} + \frac{H}{W}\left(\bar{f} - f_s\right)\right]\Big/2}}$ (20) For a Prandtl number of 0.7 $H_R = 2.24\left(\frac{W}{H}\right)^{0.1}\left(e^+\right)^{0.35}\left(\frac{\alpha}{90^o}\right)^m\left(\frac{\varepsilon_p}{10\varepsilon}\right)^n$ (21)
		Aver. Stanton number	$St_s = \bar{S}t + \frac{W}{H}(\bar{S}t - St_r)$ (22)
Pressure loss in turn ar. bend	[21]	Loss factor	$\Delta P_{TRN} = \frac{1}{2}\rho v^2 R_K$ (23)
		Comm.	$R_K = \frac{0.4}{(36.37D_h)^{0.2}}$ (24)

Tab. 1: Formulas for friction losses.

HYBRID MULTI-OBJECTIVE OPTIMIZATION

Like all single objective hybrid optimizers, multi-objective optimizers [22] are created by combining the strengths of multiple multi-objective routines. A multi-objective hybrid optimization software was created [23] using the non-dominated sorting differential evolution (NSDE) optimization algorithm, [24], strength Pareto evolutionary algorithm (SPEA), [25], multi-objective particle swarm optimization algorithm, [26], and automated switching [23] among these algorithms. The hybrid optimizer code is object oriented and written in C++. The software has been compiled and runs on MS Windows XP workstation (using Borland C++ Builder X) and Linux Workstation (GNU g++). The software begins execution by creating the population that will be used for the optimization run. The population contains the decision vector and the objective vector for all population points. The population also stores the Pareto approximation and clustering routine. Clustering is performed by the population on the object vectors of the Pareto approximation using an algorithm given by Deb [22]. Once the population has been created, the decision vectors of all population points are evenly distributed over the decision space using Sobol's pseudo random sequence [27]. The software then passes the population from optimization routine to optimization routine as the switching criteria dictates. Each routine gets a chance to work on the population until it can no longer score a grade of two or better, or the maximum limit of routine sub-iterations is reached.

VALIDATION OF MULTI-OBJECTIVE OPTIMIZER

The optimizer was tested on various standard test functions. Test results for two standard test functions, with mathematical expressions for these two test functions, are given [22, 23] as

- Poloni test function

$$\text{Poloni}\begin{cases}\text{Maximize} \quad f_1(\vec{x}) = -\left(1 + (A_1 - B_1)^2 + (A_2 - B_2)^2\right)\\ \text{Maximize} \quad f_2(\vec{x}) = -\left((x_1 - 3)^2 + (x_2 - 1)^2\right)\\ A_1 = 0.5\sin 1 - 2\cos 1 + \sin 2 - 1.5\cos 2\\ A_2 = 1.5\sin 1 - \cos 1 + 2\sin 2 - 0.5\cos 2\\ B_1 = 0.5\sin x_1 - 2\cos x_1 + \sin x_2 - 1.5\cos x_2\\ B_2 = 1.5\sin x_1 - \cos x_1 + 2\sin x_2 - 0.5\cos x_2\\ -3.1416 \le x_i \le 3.1416,\ i = 1, 2\end{cases}$$

- Kursawe test function

$$\text{Kursawe}\begin{cases}\text{Minimize} \quad f_1(\vec{x}) = \sum_{i=1}^{m-1}\left(-10\cdot e^{(-0.2)\sqrt{x_i^2 + x_{i+1}^2}}\right)\\ \text{Minimize} \quad f_2(\vec{x}) = \sum_{i=1}^{m-1}\left(|x_i|^a + 5\sin^b(x_i)\right)\\ \text{where } m = 3,\ a = 0.8,\ b = 3\\ -5 \le x_i \le 5,\ i = 1, m\end{cases}$$

The results from testing the hybrid optimizer with the Poloni problem are shown in Figure 3. In this problem there is a large discontinuity in the non-dominated set. The graph shows that by 80 function evaluations the hybrid optimizer is able to estimate the gap in the non-dominated set with satisfactory accuracy. As it can be seen in Figure 3, by 500 optimization iterations the spread of the Pareto approximation

is agreeing with the extents of the accepted non-dominated set for this problem.

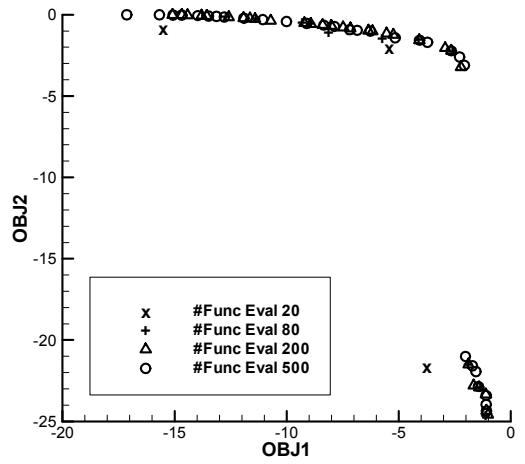

Fig. 3: Multi-objective hybrid optimizer convergence for the two-objective Poloni test optimization problem

Another problem used to test the hybrid optimizer is the Kursawe problem, Figure 4. The hybrid optimizer required at least 1500 function evaluations before an acceptable Pareto approximation could be found. This problem is more difficult than the previous problem because the population points are very close to each other in the decision space. For the results shown the magnitude of the vector (in decision space) that connects the population members with largest objective two value and the smallest objective two value is ~2.5. This means that an optimization routine that performs clustering in the decision space would have great difficulty finding a good approximation to the non-dominated set. Since the hybrid optimization software clusters in objective space this issue is avoided entirely; but the proximity of the non-dominated points in decision space still taxes the hybrid optimizer because the optimization routines in the optimizer are evolutionary. This means they can generate points outside of the region where the non-dominated set exists.

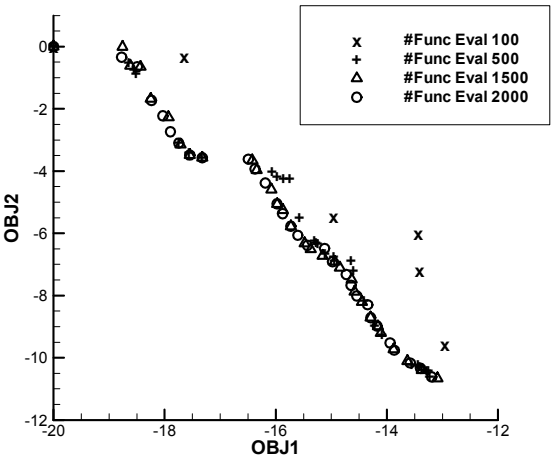

Fig. 4: Multi-objective hybrid optimizer convergence for the two-objective Kursawe test optimization problem

VALIDATION OF COOLNET

The network solver was verified by comparing the results with those obtained by Pratt and Whitney for the second rotor blade of the Pratt & Whitney F100 engine [3, 4]. Rotation speed of the blade is 13,467 rpm. The blade cross-section used for calculation is shown in Figure 1. The network of the cooling channels is shown in Figure 2. Verification is done (for Cavity 1, Cavity 2 and Cavity 3) comparing the results from COOLNET and Pratt & Whitney, this is shown in Figures 5 and 6. Cavities 1-3 are shown in Figures 1 and 2. Cavity 1 contains nodes from 25 through 31. Cavity 2 contains nodes from 22 through 38. Cavity 3 contains nodes from 39 through 47. COOLNET solved flow through the network in 45 iterations. Note that trends and magnitudes have satisfactory agreement, especially losses around 180^o bends. COOLNET predicted slightly higher mass flow rate (up to 9%). Result of this is higher pressure loss in all passages. Cause for this is probably in modeling entrance and exit hydraulic loss coefficients.

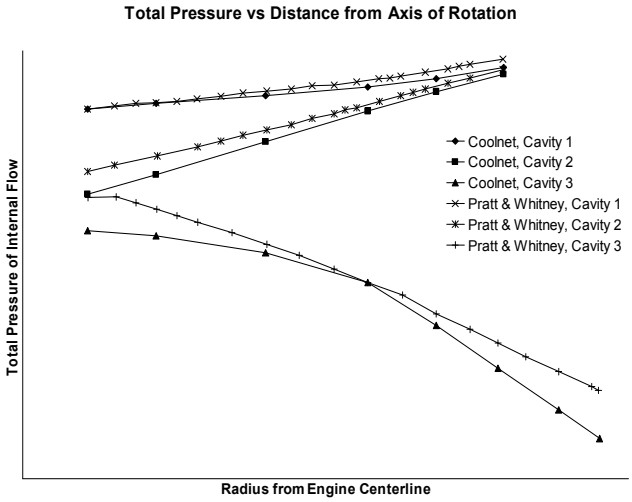

Fig. 5: Comparison of distribution of total pressures of internal coolant flow predicted by COOLNET *vs* Pratt & Whitney internal flow analysis code for F100 second blade.

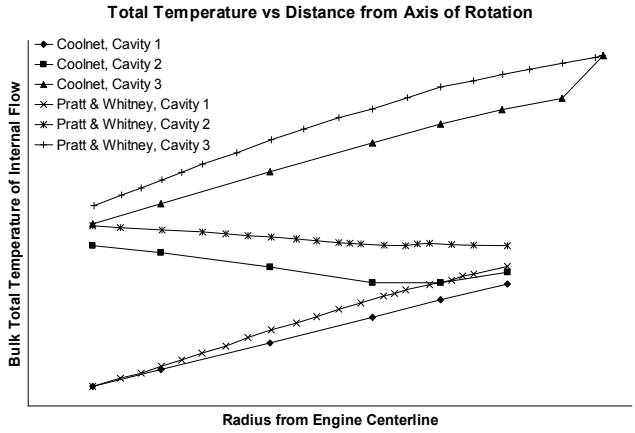

Fig. 6: Comparison of distribution of total temperatures of internal coolant flow predicted by COOLNET vs Pratt & Whitney internal flow analysis code calibrated for F100 second blade

OPTIMIZATION WITH COOLNET

Multi-objective hybrid optimizer with COOLNET was used to optimize the internal passage geometry for optimum properties. Program OBJ was written to connect optimizer and COOLNET.

Program OBJ (called by optimizer) does tasks in following way: reads COOLNET's input file, reads optimizer's output file, writes new input file for COOLNET, runs COOLNET, reads COOLNET's output file, calculates objectives, writes input file for optimizer (upon this file optimizer makes decisions). Therefore, with OBJ, the optimization process is a continuous process until variables are optimized on the objectives' basis.

Variables which are used to optimize the internal geometry of the F100 second stage turbine blade are listed in Table 2. The column labeled Name refers to which variable is being optimized. The column labeled Number refers to the amount of variables being optimized. The columns labeled Min and Max refer to the minimum and maximum variable value or the deviation in percents from the initial design used in optimization. The following list describes all the design variables taken into consideration:

- Two variables for rib angles. Cavity 1 and Cavity 2 can have different rib angles.
- Rib heights are changed for each element in Cavity 1 and Cavity 2 (Cavity 1 has six elements and Cavity 2 has six elements resulting in 12 design variables).
- Hydraulic diameters refer to the hydraulic diameter for each element. Hydraulic diameter is allowed to vary for all 48 elements independently.
- Passage cross-section areas refer to the cross-sectional area of each element. The element area is allowed to vary for all 48 elements independently.

Design variables			
Name	**Number**	**Min**	**Max**
Turbulator ribs' angle	2	25°	65°
Turbulator ribs' height	12	-20%	+20%
Hydraulic diameter	48	-15%	+15%
Passage cross-section areas	48	-15%	+15%
Total design variables	110		

Tab. 2: Design variables for the F100 2nd stage turbine blade.

Table 3 defines the optimization objectives for the F100 second stage turbine blade internal cooling passage. These objectives take in account whole blade (described by 48 elements and 47 nodes). The column labeled: Name refers to the desired objective, Number refers to the order how objectives are written for plotting, and Minimized/Maximized refers to if objective has to be minimized or maximized. Objectives are as follow:

- Total heat removed – this is heat which coolant takes out from the blade
- Total pressure drop – this is pressure drop between inlet and the exit which has the lowest pressure
- Mass flow rate – this is total mass flow rate of the coolant

Objectives			
Name	Number	Minimized	Maximized
Total heat removed	1		x
Total pressure drop	2	x	
Mass flow rate	3	x	

Tab. 3: Objectives for the F100 second stage turbine blade.

OPTIMIZED POINTS

Each optimal point in the following figures has three coordinates:

- X1- total heat removed (at Figures: max-back, min-front)
- X2 - total pressure drop (at Figures: max-left, min-right)
- X3 - mass flow rate (at Figures: max-up, min-down)

In the following figures the initial design from COOLNET is shown with a dark ball; optimized designs are shown with light balls. The purpose of these figures is to show how the optimum design variables evolve towards the best design after five hundred iterations.

There are 14 optimal points in the first iteration (Figure 7). Thus, during the first iteration the optimal points are close to the initial design.

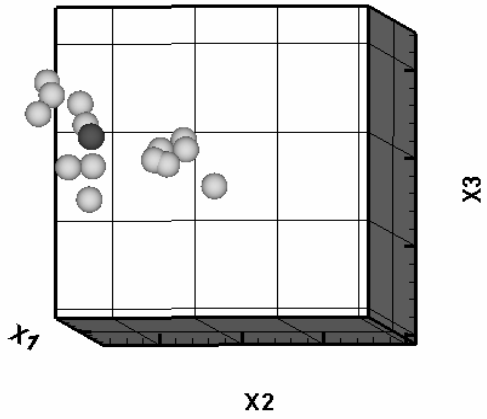

Fig. 7: Optimal points after Iteration = 1

There are 50 optimal points after the tenth iteration (Figure 8). There is progress in the optimization, compare Figure 7 and Figure 8. This figure demonstrates how the optimal design points are moving towards the optimal design.

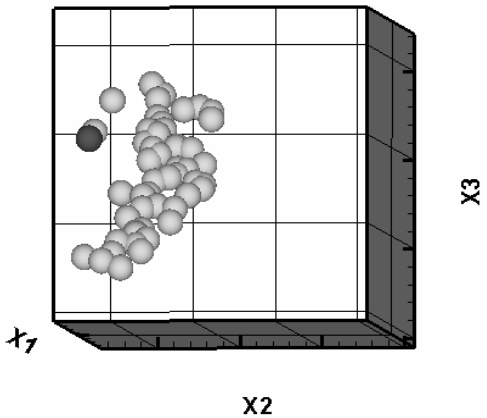

Fig. 8: Optimal points after Iteration = 10

There are 50 optimal points after the 200th iteration (Figure 9). This figure shows that with 200 iterations the optimal design points are close to the final optimal design.

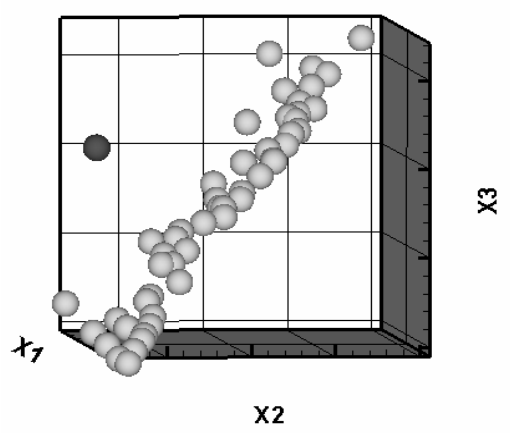

Fig. 9: Optimal points after Iteration = 200

There are 50 optimal points after the 500th iteration (Figure 10). Doing iterations after this stage will have little effect compared to the points in Figure 10, because design after 1000 iterations looks very similar to the optimized values after 500 iterations.

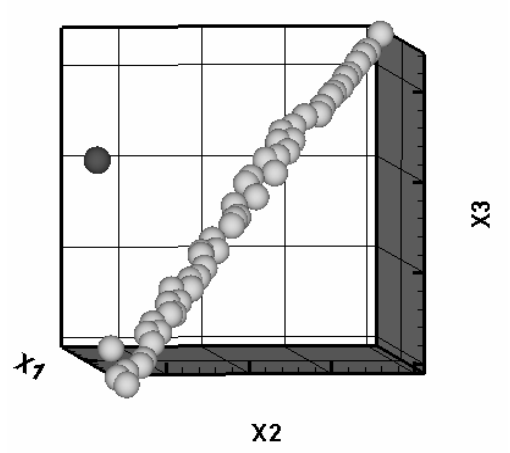

Fig. 10: Optimal points after Iteration = 500

ANALYSIS OF OPTIMIZED RESULTS

Final results to be analyzed here are based on optimal points obtained after 1,000 iterations. There are 50 optimal designs from optimization; therefore, user has to decide which represents the best his/her needs. On the basis of relative difference of each objective (for each optimal design) and the initial value for each objective, rows (R1, R2 and R3) are formed in Table 4. Row D represents the design which is obtained from the optimization (it ranges from 1 through 50). Row R1 represents total heat removed, row R2 represents total pressure drop and row R3 represents mass flow rate. These rows represent graded relative percents. Signs +/- indicate how much in percents the optimized design is better/worse compared with the starting design. TG row represents total grade, which is obtained when each of the three rows is multiplied with grade coefficient, and then they are added.

In Table 4, TG is formed with grade coefficients (1.0, 1.0, 1.0), this means that all three rows have the same importance. Depending on the: purpose of the use of the turbine blade, time for which turbine blade will be used, alloy from which the blade is made, manufacturing costs, etc. For grade coefficients can be assigned different values.

Tables 4-7 are made of 50 designs, which are grouped in 10 grading groups. Representatives from these groups are shown as columns C1-C10. Column C1 is represented with the lowest grade from its group; other columns are represented with the best grade in their group. The groups are sorted as the grade rises. This means that first group (C1) is the worst and the tenth group (C10) is the best..

From Table 4 it can be seen that for grade coefficients (1.0, 1.0, 1.0) the best design is in column C10 with total grade 8.8. Only for this grading case, it can be said that this design D = 47 is overall 8.8% better than the initial design.

	C1	C2	C3	C4	C5	C6	C7	C8	C9	C10
D	49	9	23	21	3.0	17	16	15	20	47
R1	-24.6	-15.7	-11.1	-7.7	-4.2	1.5	6.4	4.0	13.1	14.9
R2	-0.6	0.9	1.4	1.8	2.2	2.9	3.5	3.2	4.2	4.5
R3	26.0	18.2	13.8	10.5	7.2	2.1	-2.8	0.1	-9.0	-10.6
TG	0.9	3.4	4.0	4.6	5.2	6.5	7.1	7.3	8.3	8.8

Tab. 4: Optimal designs with grade coefficients (1.0, 1.0, 1.0)

Table 5 is formed with grade coefficients (1.25, 0.5, 1.25). In this case three objectives are not with the same importance. With higher importance are the total heat removed and mass flow rate; less important is the total pressure drop. For this grading case the best design is D = 47 with total grade 7.6.

	C1	C2	C3	C4	C5	C6	C7	C8	C9	C10
D	49	9	25	38	3	17	16	7	24	47
R1	-24.6	-15.7	-13.8	-5.1	-4.2	1.5	6.4	8.0	17.7	14.9
R2	-0.6	0.9	1.1	1.9	2.2	2.9	3.5	3.6	4.7	4.5
R3	26.0	18.2	16.6	7.9	7.2	2.1	-2.8	-4.3	-13.9	-10.6
TG	1.5	3.6	4.1	4.4	4.9	6.0	6.2	6.4	7.0	7.6

Tab. 5: Optimal designs with grade coefficients (1.25, 0.5, 1.25)

Table 6 is formed with grade coefficients (1.5, 0.75, 0.75). This means that total heat removed is considered more important than pressure drop and mass flow rate. For this grading case the best design is D = 48 with total grade 20.1.

	C1	C2	C3	C4	C5	C6	C7	C8	C9	C10
D	49	9	13	21	39	17	6	32	42	48
R1	-24.6	-15.7	-11.9	-7.7	-3.3	1.5	6.0	8.9	14.0	18.4
R2	-0.6	0.9	1.3	1.8	2.0	2.9	3.4	3.8	4.2	4.7
R3	26.0	18.2	14.8	10.5	6.3	2.1	-2.3	-5.6	-10.1	-14.8
TG	-17.8	-9.2	-5.8	-2.3	1.3	6.0	9.8	11.9	16.7	20.1

Tab. 6: Optimal designs with grade coefficients (1.5, 0.75, 0.75)

Table 7 is formed with grade coefficients (0.5, 1.0, 1.5). Here, total heat removed is considered less important than pressure drop and less important than mass flow rate. For this case the best design is D = 49 with total grade 26.2. However, total heat removed for this design decreased by 24.6.

	C1	C2	C3	C4	C5	C6	C7	C8	C9	C10
D	48	22	16	1	10	11	23	19	41	49
R1	18.4	9.7	6.4	2.4	-2.6	-6.9	-11.1	-15.2	-20.1	-24.6
R2	4.7	3.6	3.5	3.0	2.3	1.8	1.4	0.9	0.1	-0.6
R3	-14.8	-6.2	-2.8	1.5	5.7	9.8	13.8	17.9	22.2	26.0
TG	-8.32	-0.8	2.47	6.43	9.48	13.0	16.5	20.1	23.3	26.2

Tab. 7: Optimal designs with grade coefficients (0.5, 1.0, 1.5)

In conclusion, the suggested user-specified grading of the individual optimized objectives does not lead to the most desired design if constraints are not applied for totally not desired values.

Design D = 47 will be compared with the initial design for F100 second stage turbine blade. Program PLOT is written to read input and output file from COOLNET. PLOT's main purpose is to generate input file for Tecplot 10, with optimized (or initial) geometry and desired value (total pressure, static pressure, Mach number, Reynolds number, mass flow rate, total temperature, static temperature) which is to be plotted in the passage. In the following plots width is hydraulic diameter of the element, and length is length of the element. X2 axis minimum/ maximum represents minimum/maximum radius.

Mass flow rate for starting geometry is shown in Figure 11. For D = 47 geometry mass flow rate is shown at Figure 12. Same colors represent same local mass flow rate values in both figures. Also, it can be seen how hydraulic diameters have changed by comparing the two figures. Values difference in legend (between min and max value) is low so, nuances can be seen easily for mass flow rate – this is the reason why both Figure 11 and 12 are shown. It can be seen that optimized design D = 47 has slightly increased mass flow rate compared to initial design. This can be seen also in Table 4.

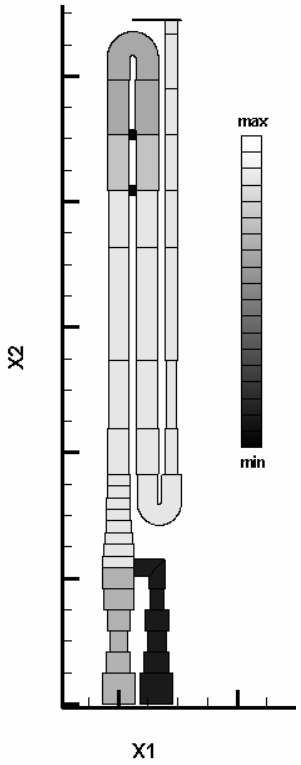

Fig. 11: Mass flow rate variation for initial geometry

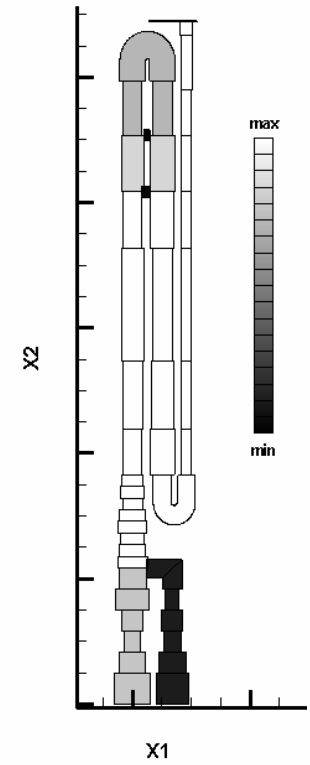

Fig. 12: Mass flow rate variation for D = 47 optimized geometry

Note that in legend (for Figures 13, 15 and 17) index s means starting geometry, and index o means optimized D = 47 geometry.

Figure 13 is introduced to show difference in mass flow rate for initial geometry and for optimized D = 47 geometry in the cavities. Some explanations for better understanding of Figure 13: flow in Cavity 1 is shown from very left and then through inclined line, flow in Cavity 2 is shown through inclined line till very left and flow in Cavity 3 is shown from very left to very right. Inclined lines (which are going down) present flow in elements E27 and E28 (or E31 and E32). Difference in vertical direction among horizontal lines and these inclined lines represent mass flow rate in elements E29 and E26.

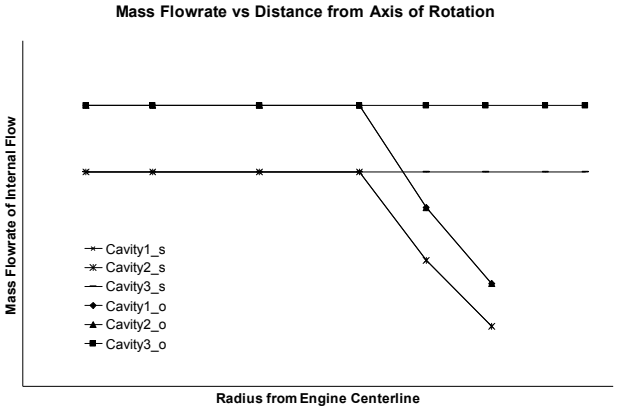

Fig. 13: Mass flow rates for initial geometry and for D = 47 optimized geometry in the main cavities

Total temperature for D = 47 optimized geometry is shown in Figure 14. Change in colors can not be seen because difference in values in legend (between min and max value) is high, then nuances cannot be seen easily for total temperature – this is the reason why the initial design is not shown.

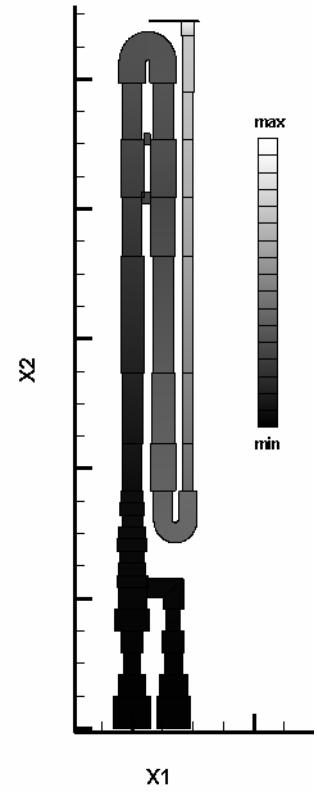

Fig. 14: Total temperature variations for D = 47 optimized geometry

Figure 15 is introduced to show difference in total temperature for starting geometry and for optimized D = 47 geometry in the main cavities. It can be seen that D = 47 has higher exit total temperatures compared to the initial design although inlet in Cavity 1 is with the same total temperature. This can also be seen in Table 4.

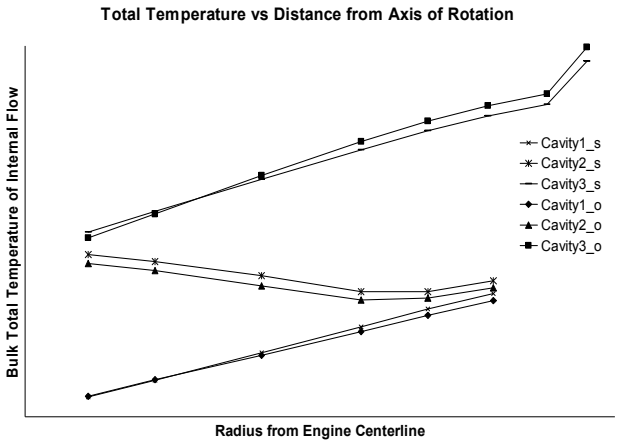

Fig. 15: Total temperature variation for initial and D = 47 optimized geometry in the main cavities

Total pressure for D = 47 optimized geometry is shown in Figure 16. Change in colors cannot be seen because the difference in values in legend (between min and max value) is not large, but percentage of improvement is 4.5%; so, nuances in gray scale cannot be seen easily for total pressure. This is the reason why the initial design is not shown.

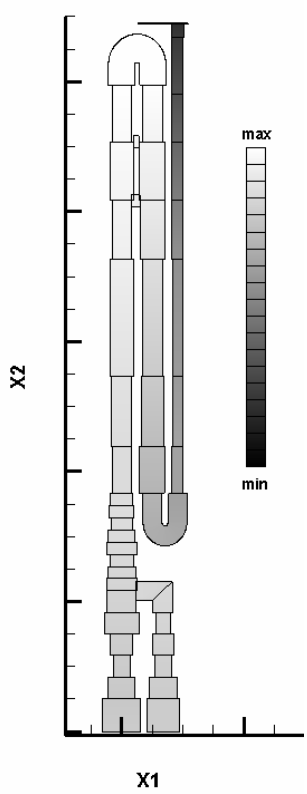

Fig. 16: Total pressure variation for D = 47 optimized geometry

Figure 17 is introduced to show the difference in total pressure for starting geometry and for the optimized D = 47 geometry in the main cavities. It can be seen that D = 47 has higher total pressures compared to starting design, through all three cavities. This can be seen also in Table 4.

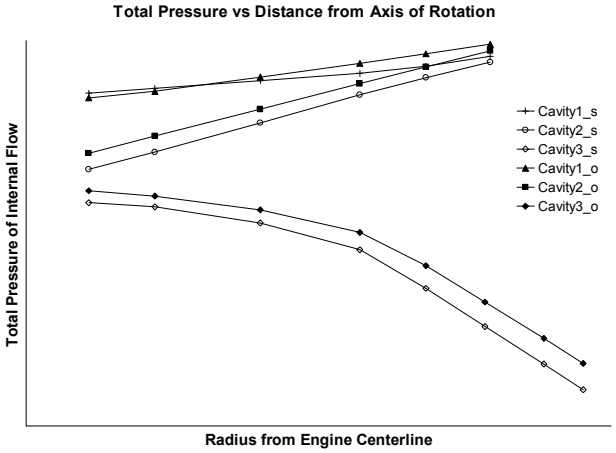

Fig. 17: Total pressure variation for starting and D = 47 optimized geometry in the main cavities

Figure 18 shows that optimum design D = 47 has rib angles of 33.6 degrees for Cavity 1 and 35.6 degrees for Cavity 2, compared to initial design which has turbulator ribs inclined at 45 degree from normal to the local flow in both cavities.

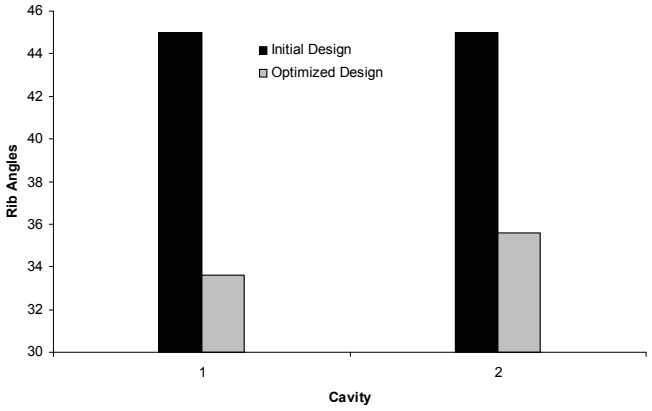

Fig. 18: Turbulator ribs' angles for initial and D = 47 optimized geometry

Figure 19 compares optimum case D = 47 and initial case. In Cavity 1 it shows that optimum case D = 47 has turbulator ribs' heights below the values used in the initial design. In Cavity 2 it shows that for optimum case D = 47 the inlet has lower and that the exit has higher ribs' heights compared to the values in the initial design.

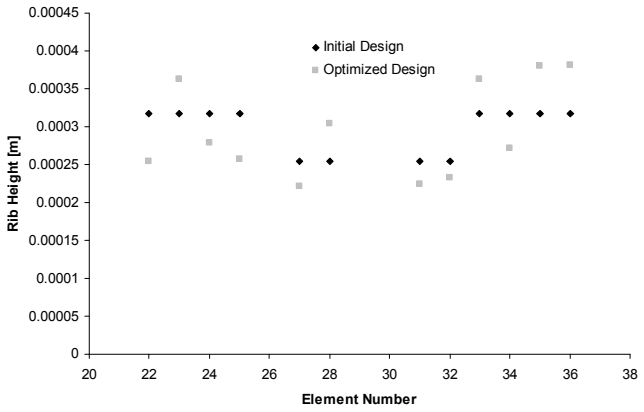

Fig. 19: Turbulator ribs' heights for initial and D = 47 optimized geometry

Figure 20 compares cross-sectional areas of the elements for initial and D = 47 optimized geometry. This figure shows that optimum case D = 47 has mostly smaller cross section areas before Cavity 1 and after that mostly higher cross-section areas compared to the initial design.

Figure 21 compares hydraulic diameters of the elements for initial and D = 47 optimized geometry. It shows that optimum case D = 47 has oscillatory smaller and larger hydraulic diameters of the elements before Cavity 3 and in Cavity 3 smaller hydraulic diameters of the elements, compared to the initial design.

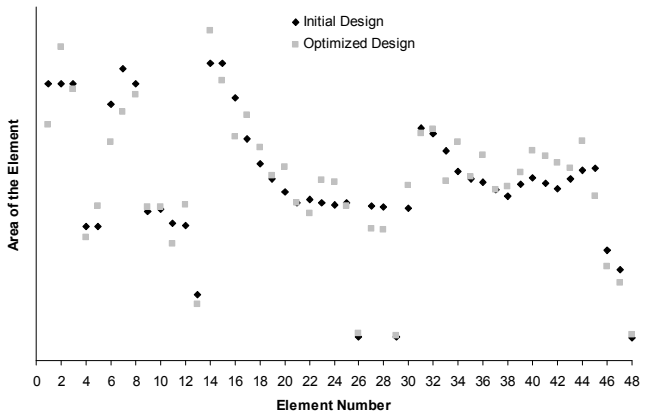

Fig. 20: Cross-sectional areas of the elements for initial and D = 47 optimized geometry

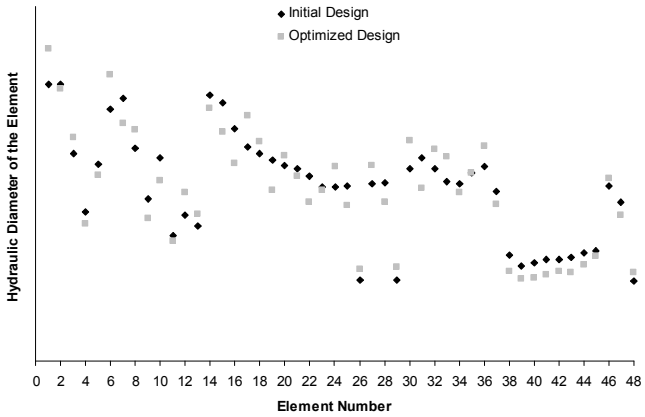

Fig. 21: Hydraulic diameters of the elements for initial and D = 47 optimized geometry

CONCLUSIONS

A methodology and accompanying software for preliminary multi-objective design optimization of branching internal cooling passages utilizing a compressible homocompositional fluid have been described and demonstrated. The software package includes: a multi-objective hybrid optimizer, COOLNET (quasi 1-D thermo-fluid analysis code), OBJ and PLOT (graphics interface).

COOLNET analysis software has the same trends as shown in an earlier publication depicting the results of a similar analysis code used by Pratt & Whitney. Hybrid multi-objective optimization code was verified against classical test cases involving two objectives. COOLNET needs approximately 50 iterations to analyze each configuration. Hybrid multi-objective optimizer needs approximately 500 iterations to create a converged Pareto front of optimized design configurations. The entire design optimization process required approximately 15,000 analysis runs and consumed seventeen hours on a 3.0GHz Pentium 4 double processor.

After finding the Pareto front points, the user has to decide which point is the best. It was demonstrated that this could be accomplished by creating a composite grading formula where each individual objective function value in the optimized design is graded by a user-specified coefficient.

In this article, the final Pareto front had 50 optimized configurations. Using this composite grading formula, configuration D = 47 was found to have the best total grade in two cases, that is, the maximum amount of heat removed and the minimal total pressure drop, while having only a slightly higher coolant mass flow rate.

REFERENCES

1. Alhabri, A. Y., Pence, D. V. and Cullion, R. N., 2003, "Temperature Distributions in Microscale Fractal-like Branching Channel Networks", ASME paper HT2003-47501, ASME Summer Heat Transfer Conference, Las Vegas, NV, July 21-23, 2003.
2. Martin, T. J., 2001, "Computer-Automated Multi-Disciplinary Analysis and Design Optimization of Internally Cooled Turbine Blades," Ph.D. Dissertation, Department of Aerospace Engineering, The Pennsylvania State University, University Park, PA.
3. Martin, T. J. and Dulikravich, G. S., 2001, "Aero-Thermo-Elastic Inverse Design and Optimization of Internally Cooled Turbine Blades", Chapter 5 in *Coupled Field Problems, Series on Advances in Boundary Elements,* (eds: Aliabadi, M. H. and Kassab, A. J.), WIT Press, Boston, MA, pp. 137-184.
4. Martin, T. J. and Dulikravich, G. S., 2002, "Analysis and Multi-Disciplinary Optimization of Internal Coolant Networks in Turbine Blades", *AIAA Journal of Propulsion and Power*, Vol. 18, No. 4, pp. 896-906.
5. Martin, T. J., Milliken, A., Pack. D. and Hummel, R. S., 2004, "Using a Parametric, Feature-Based Engineering Environment for the Design, Transient Thermal-Stress Analysis, and Life Assessment of Cooled Turbine Airfoils", ASME paper IMECE2004-62308, Anaheim, CA, Nov. 15-21, 2004.
6. Brillert, D., Reichert., A. W. and Simon H., 1999, "Calculation of Flow Losses in Rotating Passages of Gas Turbine Cooling Systems", ASME paper 99-GT-251, International Gas Turbine & Aeroengine Congress & Exposition, Indianapolis, IN, June 7-10, 1999.
7. Visser, J. A., 1999, "A Simplified Equation to Obtain the Complex Heat Transfer Distribution in an Internal Duct of a Semi-Cooled Turbine Blade", ASME paper 99-GT-13, International Gas Turbine & Aeroengine Congress & Exposition, Indianapolis, IN, June 7-10, 1999.
8. Florschuetz L. W. and Metzger D. E., 1984, "Effects of Initial Crossflow Temperature on Turbine Cooling with Jet Arrays", *Heat and Mass Transfer in Rotating Machinery*, pp. 499-510.
9. Bejan, A., 1997, "Constructal Tree Network for Fluid Flow Between a Finite-Size Volume and One Source or Sink", *Revue Generale de Thermique*, Vol. 36, pp. 592-604.
10. Han, Z.-X., Dennis, B. H. and Dulikravich, G. S., 2001, "Simultaneous Prediction of External Flow-Field and Temperature in Internally Cooled 3-D Turbine Blade Material," *International Journal of Turbo & Jet-Engines*, Vol. 18, No. 1, pp. 47-58.
11. Kawaike, K., Shunichi, A. and Sasada, T., 1992, "Integrated CAE System for Cooled Turbine Blade Design and Verification Tests of Analytical Codes", *Proceedings of International Symposium on Heat Transfer in Turbomachinery*, (eds: Goldstein, R. J., Metzger, D. E. and Leontiev, A. I.), Athens, Greece, August 1992, pp. 73-84.
12. Gritsch, M., Schulz, A. and Wittig, S., 1997, "Discharge Coefficient Measurements of Film-Cooling Holes With Expanded Exits", ASME Paper 97-GT-165, International Gas Turbine & Aeroengine Congress & Exhibition, Orlando, FL, June 2-5, 1997.
13. Moaveni, S., 2003, *Finite element analysis: theory and application with ANSYS*, 2nd Edition, Pearson Education, Upper Saddle River, NJ.
14. Reddy, J. N., and Gartling, D. K., 2000, *The Finite Element Method in Heat Transfer and Fluid Dynamics*, 2nd Edition, CRC Press, Boca Raton, FL.
15. Press, W. H, Teukolsky, S. A., Vetterling, W. T. and Flannery, B. P., 1986, *Numerical Recipes in FORTRAN, The Art of Scientific Computing*, 2nd Edition, Cambridge University Press, Cambridge, UK.
16. Haaland, S. E., 1983, "Simple and Explicit Formulas for the Friction Factor in Turbulent Pipe Flow", *ASME Journal of Fluids Engineering*, Vol. 105, pp. 89-90.
17. Dipprey, D. F. and Sabersky, R. H., 1963, "Heat and Momentum Transfer in Smooth and Rough Tubes at Various Prandtl Numbers", *International Journal of Heat and Mass Transfer*, Vol. 6, pp. 329-353.
18. Schlichting, H., 1979, *Boundary Layer Theory*, Translated by Kestin, J., McGraw Hill Book Co., New York, NY.
19. Han, J. C., and Park, J. S., 1988, "Developing Heat Transfer in Rectangular Channels with Rib Turbulators", *International Journal of Heat and Mass Transfer*, Vol. 31, No. 1, pp. 183-195.
20. Webb, R. L., 1998, *Principles of Enhanced Heat Transfer*, John Wiley & Sons, Inc., New York, NY.
21. White, F. M., 1988, *Heat and Mass Transfer*, Addison-Wesley, Reading, MA.
22. Deb, K., 2002, *Multi-Objective Optimization Using Evolutionary Algorithms*, John Wiley & Sons.
23. Dulikravich, G. S., Moral, J. R. and Sahoo, D., 2005, "A Multi-Objective Evolutionary Hybrid Optimizer", EUROGEN 05 - Evolutionary and Deterministic Methods for Design, Optimisation and Control with Applications to Industrial and Societal Problems, Munich, Germany, September 12-14, 2005.
24. Iorio, A. and Li, X., 2004, "Solving Rotated Multi-objective Optimization Problems Using Differential Evolution", *Proceeding of the 17th Joint Australian Conference on Artificial Intelligence*.
25. Zitzler, E. and Thiele, L., 1999, "Multiobjective Evolutionary Algorithms: A Comparative Case Study and the Strength Pareto Approach" *IEEE Transactions on Evolutionary Computation*, Vol. 3, No. 4, pp. 257-271.
26. Eberhart, R., Shi, Y. and Kennedy, J., 2001, *Swarm Intelligence*, Morgan Kaufmann.
27. Sobol, I. M., 1976, "Uniformly Distributed Sequences with an Additional Uniform Property", *USSR Computational Mathematics and Mathematical Physics*, Vol. 16, pp. 236-242.